

Multi-Modal MRI Reconstruction Assisted with Spatial Alignment Network

Kai Xuan, Lei Xiang, Xiaoqian Huang, Lichi Zhang, Shu Liao, Dinggang Shen, and Qian Wang

Abstract—In clinical practice, magnetic resonance imaging (MRI) with multiple contrasts is usually acquired in a single study to assess different properties of the same region of interest in human body. The whole acquisition process can be accelerated by having one or more modalities under-sampled in the k -space. Recent researches demonstrate that, considering the redundancy between different contrasts or modalities, a target MRI modality under-sampled in the k -space can be more efficiently reconstructed with a fully-sampled MRI contrast as the reference modality. However, we find that the performance of the above multi-modal reconstruction can be negatively affected by subtle spatial misalignment between different contrasts, which is actually common in clinical practice. In this paper, to compensate for such spatial misalignment, we integrate the spatial alignment network with multi-modal reconstruction towards better reconstruction quality of the target modality. First, the spatial alignment network estimates the spatial misalignment between the fully-sampled reference and the under-sampled target images, and warps the reference image accordingly. Then, the aligned fully-sampled reference image joins the multi-modal reconstruction of the under-sampled target image. Also, considering the contrast difference between the target and the reference images, we particularly design the cross-modality-synthesis-based registration loss, in combination with the reconstruction loss, to jointly train the spatial alignment network and the reconstruction network. Experiments on both clinical MRI and multi-coil k -space raw data demonstrate the superiority and robustness of multi-modal MRI reconstruction empowered with our spatial alignment network. Our code is publicly available at <https://github.com/woxuankai/SpatialAlignmentNetwork>.

Index Terms—Image Synthesis, Magnetic Resonance Imaging, MRI Reconstruction, Multi-Modal Reconstruction, Multi-Modal Registration

I. INTRODUCTION

The magnetic resonance (MR) imaging, or simply MRI, is a non-invasive and radiation-free imaging technology that has been widely used in clinical practice. However, limited by the device and imaging protocols, MR scan is relatively slow, and the acceleration of MRI acquisition has been an important and everlasting research topic since its invention. A feasible remedy is to exploit the redundancy between signals received from different coils in parallel imaging [1], [2]. Also,

compressed sensing MRI (CS-MRI) [3] allows for accurate reconstruction from the signals that are highly sparse in the k -space with respect to the Nyquist-Shannon sampling criterion.

Aside from accelerating MRI acquisition by exploiting the intrinsic redundancy within a single MR image, the common information coupled and shared by different MRI sequences draws a lot of attention. In clinical practice, MR images of different contrasts are usually acquired in the same study to reflect different properties of the same region of interest (ROI) and to facilitate precise diagnosis. Recent researches [4], [5] demonstrate that multi-modal MRI reconstruction is capable of restoring the partially acquired MR sequence (i.e., the *target modality*) with auxiliary input from another fully-sampled *reference modality* in the same study. With the target acquisition under-sampled in the k -space, the overall time cost of the whole study in MR scanning can thus be reduced.

However, we find that the spatial misalignment between modalities, though may be subtle and previously ignored, can non-negligibly weaken the final reconstruction quality of the target modality. Such spatial misalignment is prevalent between individual sequences of the same study. A real example can be found in Fig. 1(a), where the consecutively acquired T1-weighted and T2-weighted images from the same subject are shown. One may easily notice the misalignment of the corresponding anatomic structures as highlighted by arrows.

The reason behind such misalignment can be complex. Although the subjects are typically instructed to keep still during MRI acquisition, a person even without any MRI knowledge can easily notice the gap between two sequences, e.g., due to pause and altered noises of the scanner. Thus, one may then tend to relax and have tiny movement, which can lead to subtle yet mostly inevitable motion between the sequences, even though external stabilization measures are usually deployed.

Few literature noticed this issue of spatial misalignment between MRI modalities of the same study. With CS-MRI, Lai *et al.* [6] proposed to register the reference modality to the mono-contrast reconstruction of the target modality, as the reference image cannot be directly registered to zero-filled target MRI. Meanwhile, in the recent deep learning era, most reported experiments of multi-modal MRI reconstruction are conducted on carefully registered multi-contrast MRI [7]–[10]. Although pre-processing can effectively suppress the misalignment for training and validation in labs, such issues can hardly be avoided in real scenario.

Enlarging model capacity with a deeper neural network is a universal solution towards better performance, but it lacks insight about the spatial misalignment issue and suffers

Kai Xuan, Lei Xiang, Lichi Zhang, and Qian Wang are with School of Biomedical Engineering, Shanghai Jiao Tong University, Shanghai 200030, China (e-mail: {kaixuan, xianglei_15, lichizhang, wang.qian}@sjtu.edu.cn).

Xiaoqian Huang and Shu Liao are with Shanghai United Imaging Intelligence Co., Ltd., Shanghai 200230, China (e-mail: {xiaoqian.huang, shu.liao}@united-imaging.com)

Dinggang Shen is with School of Biomedical Engineering, ShanghaiTech University, Shanghai 201210, China. He is also with Shanghai United Imaging Intelligence Co., Ltd., Shanghai 200230, China and Department of Artificial Intelligence, Korea University, Seoul 02841, Republic of Korea (e-mail: dinggang.shen@gmail.com).

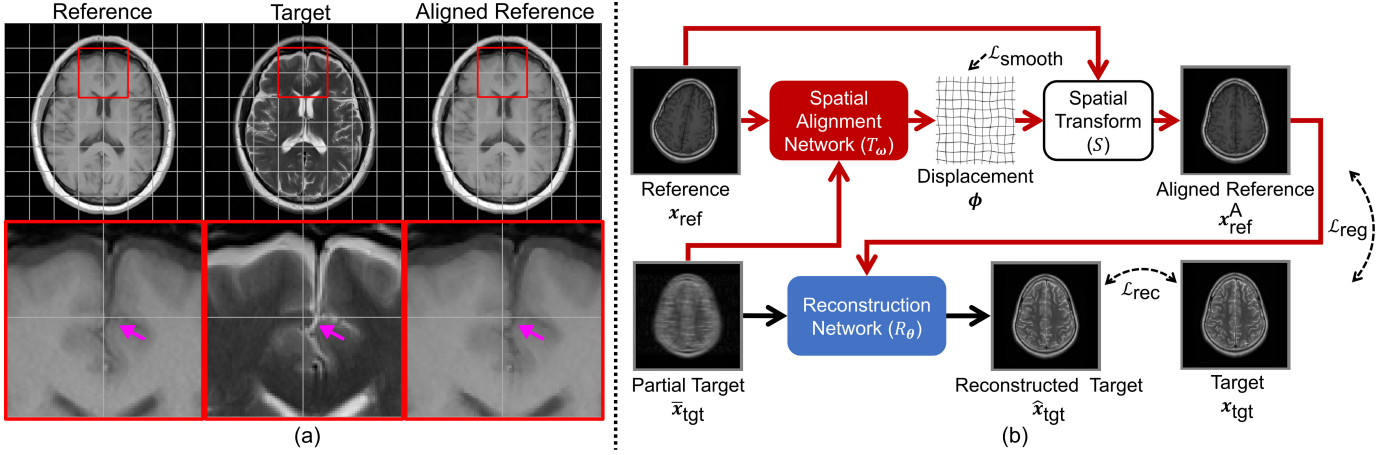


Fig. 1. A real case demonstrating the existence of spatial misalignment (a), and the overview of the proposed method (b). In (a), a real case of multi-modal MRI acquired for the diagnostic purpose demonstrates the existence of spatial misalignment (highlighted by arrows) between the reference (T1-weighted) and the target (T2-weighted) images. The aligned reference image is also available to show the effect of our proposed spatial alignment network. In (b), a spatial alignment network is integrated into the multi-modal MRI reconstruction pipeline to compensate for the spatial misalignment between the fully-sampled reference image and the under-sampled target. The data flow for the conventional deep-learning-based reconstruction is shown in black arrows; and the red arrows are for additional data flow related to our proposed spatial alignment network.

from diminishing marginal utility in multi-modal reconstruction [11]. Alternatively, in this work, we propose an effective solution to explicitly mitigate the negative impact of the spatial misalignment. Particularly, we use a plug-in spatial alignment network to align the reference MRI with the zero-filled target image, in combination with the multi-modal MRI reconstruction network. An overview of our proposed method is shown in Fig. 1(b). First, the spatial alignment network is employed to estimate the motion between the fully-sampled reference MRI and the under-sampled target. Then, the warped reference image, instead of the misaligned original one, is concatenated with the under-sampled target and fed into the reconstruction network, which is then able to yield the high-quality target image.

Our contributions can be summarized as follows:

- We propose to compensate for the subtle spatial misalignment between the reference and the target modalities explicitly in multi-modal MRI reconstruction.
- To optimize the spatial alignment network, aside from training with the image reconstruction loss, the combination of the cross-modality-synthesis-based loss further improves the registration and the reconstruction quality.
- Finally, the proposed method demonstrates superior performance on both clinical MRI and raw k -space data.

II. RELATED WORKS

In this section, we first introduce the development of MRI reconstruction in Section II-A, and then the idea of improving target image reconstruction quality with auxiliary information from the reference images in Section II-B. Finally, we discuss multi-modal medical image alignment in Section II-C.

A. MRI Reconstruction

To recover fully-sampled MR images from partially acquired k -space signals, image reconstruction plays a key role especially concerning the final image quality. Basic solutions

including linear filtering or zero-filling are used to recover the missing k -space signals, while those relatively simple methods tend to bring in artifacts in the reconstructed MR images as the requirement of Nyquist-Shannon sampling theorem is not fully met. Compressed sensing (CS) [12] and its application to MRI [3] are the milestone of under-sampled MRI reconstruction, as it can restore MR images from sparse k -space signals. The technique has effectively accelerated MRI acquisition.

Deep learning has become a latest breakthrough in MRI reconstruction. In the pilot work of Wang *et al.* [13], a convolutional neural network (CNN) is trained offline to model the mapping from zero-filled under-sampled MR images to the corresponding fully-sampled ones. Later, the techniques such as data consistency layers [14] and recurrent neural networks (RNNs) [15] are used to further improve the reconstruction quality. While most works follow the image-space modeling paradigm used in CS-MRI, Han *et al.* [16] proposed to estimate the missing MR signals in the k -space where MRI is physically acquired. Further, Zhang *et al.* [17] processed MRI signals on both image space and k -space. Another interesting deep-learning-based solution for MRI reconstruction is to directly estimate the fully-sampled MR images from partially acquired k -space signals without referring to Fourier transform explicitly [18].

B. Reference-based MRI Reconstruction

With physiology-related redundancy between MR images, reconstructing under-sampled MRI with auxiliary information from reference images is a promising way. Regarding multiple visits of the same patient, Souza *et al.* [19] proposed to accelerate MRI follow-ups with early intra-subject images. Weizman *et al.* [20], [21] proposed a more flexible solution in that they also support the case when the reference is not fully available. Schlemper *et al.* [14] took advantage of the redundancy between adjacent temporal frames of dynamic MRI and used the 3D convolutional operation (2D + time)

to learn their temporal correlation. Moreover, the redundancy between spatially neighboring 2D slices in a 3D volume was used in Hirabayashi *et al.* [22], to improve the reconstruction quality by conducting full sampling every several slices while under-sampling the rest. For each under-sampled slice, rather than estimating the slice directly, they estimated the difference between the current slice and the neighboring fully-sampled one. Also note that multi-modal reconstruction is not only limited to MRI. The idea has been successfully used in various tasks, e.g., enhancing low-dose positron emission tomography (PET) quality with corresponding MRI to reduce the radiation risk of PET/MRI scanning [23].

The reconstruction of a certain MRI modality can be enhanced with the helps from other modalities, as a typical MRI study consists of multiple sequences and they are usually acquired sequentially. Majumdar *et al.* [24] and Huang *et al.* [25] jointly reconstructed T1-/T2-weighted images of the same ROI from under-sampled MRI signals. For learning-based methods, Song *et al.* [26] proposed coupled dictionary learning for multi-contrast MRI reconstruction. More recently, with deep neural networks, Kim *et al.* [5] and Xiang *et al.* [4] proposed to speed up T2-weighted acquisition by integrating T1-weighted image as the reference into the reconstruction process. More techniques, such as progressive neural network [9], generative adversarial network [10], and dilated convolution [8], are also investigated to improve multi-modal MRI reconstruction.

C. Multi-Modal MRI Alignment

Image registration is a classical topic in medical image analysis, and it is developing fast nowadays when enabled with deep learning. Traditional methods take registration as an optimization problem, and the displacement field is optimized iteratively with an objective function consisting of the image similarity loss and the regularization term. Such methods are popular, including ANTs [27], Demons [28], [29], and SPM [30]. In the alternative learning-based methods, especially for deep-learning-based registration, the complex displacement field can be directly learned between the fixed and the moving images. Early works train deep neural networks to predict the displacement fields in a supervised manner [31]. Later, unsupervised training is proposed to improve the flexibility and performance of deep-learning-based registration [32].

It is critical to design accurate and robust metric to quantify image similarity, especially for the case of multi-modal or multi-contrast registration. However, the metric is challenging to design in computer vision due to the huge appearance gap across different image modalities. Mutual information (MI), describing the pixel- or voxel-wise statistical dependence between corresponding intensities of the images to be aligned [33], has been successfully applied to various multi-modal image registration tasks, e.g., PET-computed tomography (CT) alignment [34], and PET-MRI registration [35]. Later, feature-based similarity metrics such as modality independent neighborhood descriptor (MIND) [36] take use of high-order appearance features to establish spatial correspondences. With deep learning, Fan *et al.* [37] proposed to

measure the image similarity with the generative adversarial network (GAN), but paired images were required in their work as positive examples for training. Cao *et al.* [38] circumvented the direct similarity measurement with cross-modality synthesis. They thus could replace the difficult calculation of multi-modal similarity with a much simpler mono-modal metric. Further, to prevent possible spatial distortion introduced by cross-modality synthesis, the geometric-preserving technique was adopted in Arar *et al.* [39].

III. METHODS

The framework of our proposed method is illustrated in Fig. 1(b). It includes (1) the spatial alignment network to register the reference image with the partially sampled target, and (2) the reconstruction network to restore the target modality image of high quality. There are three major loss functions that play critical roles in our framework. Other than the commonly used smoothness constraint $\mathcal{L}_{\text{smooth}}$ upon the displacement field, we also calculate the reconstruction loss \mathcal{L}_{rec} and the registration loss \mathcal{L}_{reg} to train the spatial alignment network and the reconstruction network jointly.

The rest of Section III will be arranged as follows. Section III-A presents the mathematical formulation of multi-modal MRI reconstruction aided by the spatial alignment network. Then, the three loss functions, i.e., the smoothness constraint $\mathcal{L}_{\text{smooth}}$, the reconstruction loss \mathcal{L}_{rec} and the registration loss \mathcal{L}_{reg} , are described in Section III-B. Finally, in Section III-C, we introduce more implementation details.

A. Multi-Modal MRI Reconstruction

In this subsection, we first formulate the learning-based MRI reconstruction, and then introduce the multi-modal MRI reconstruction. Next, we discuss how to integrate the proposed spatial alignment network into the multi-modal MRI reconstruction pipeline.

1) *MRI Reconstruction:* The MRI acquisition can be perceived as sampling in a full k -space. Taking 2D MRI of the image shape of $N_x \times N_y$ for example, with a flattened complex-valued fully-sampled MRI image $\mathbf{x} \in \mathbb{C}^N$ where $N = N_x \times N_y$, the fast MRI acquisition process can be expressed as $\mathbf{y} = \mathbf{F}_u \mathbf{x}$, where $\mathbf{y} \in \mathbb{C}^M$ is the (partially) sampled MR signals in the k -space with the sampling ratio $\frac{M}{N}$, ($M \leq N$). $\mathbf{F}_u \in \mathbb{C}^{M \times N}$, being consistent with notations in Lustig *et al.* [3], is a matrix representing the whole MRI under-sampling process which usually consists of the Fourier transform and the k -space under-sampling. Note that the number of coils is ignored here for simplicity, though the above formulation can be easily extended to the multi-coil setting.

Without loss of generality, the deep-learning-based MRI reconstruction method employs a neural network R with parameters θ to estimate the fully-sampled MRI \mathbf{x} from the under-sampled k -space signals \mathbf{y} . Before feeding to the deep network, usually the raw acquisition \mathbf{y} is pre-processed with $\mathbf{F}_{0-\text{fill}}^{-1} \in \mathbb{C}^{N \times M}$, which represents zero-filling of the missing MR signals and inverse Fourier transform to map the k -space data back to the image space. In this way, one can have the

under-sampled MR image $\bar{x} = F_{0-\text{fill}}^{-1}y$, $\bar{x} \in \mathbb{C}^N$. Next, as aliasing typically exists in \bar{x} , the reconstruction network R_θ should be capable of restoring the fully-sampled MRI from the under-sampled one, i.e., $\hat{x} = R_\theta(\bar{x})$.

2) *Multi-Modal MRI Reconstruction*: The target MR image x_{tgt} can be better reconstructed with the helps of the reference, such as an image of the same ROI yet of different contrast acquired in the same study. Extracting common information from the reference image of a different contrast is non-trivial. And in the context of deep learning, this process is expected to be completed in a sophisticated data-driven and encoding-decoding way.

In early works [4], [5], the fully-sampled reference modality x_{ref}^A and the under-sampled target modality \bar{x}_{tgt} are concatenated in the channel dimension, and fed into a single reconstruction network R_θ . It is expected that x_{ref}^A can help reconstruct x_{tgt} then, as the network should fuse individual channels of inputs and feature maps through forward convolution. As a summary, the multi-modal MRI reconstruction process can be formulated as $\hat{x}_{\text{tgt}} = R_\theta(\bar{x}_{\text{tgt}}, x_{\text{ref}}^A)$. The superscript A of x_{ref}^A indicates that the reference image is well-aligned to the target modality virtually.

3) *Spatial Alignment Network*: In this work, we propose to integrate a spatial alignment network T_ω into the multi-modal MRI reconstruction, in order to estimate and compensate for the subtle spatial misalignment between the target and the reference modalities. First, the spatial alignment network explicitly estimates the displacement field ϕ between the under-sampled target modality \bar{x}_{tgt} and the fully-sampled reference modality x_{ref} following

$$\phi = T_\omega(\bar{x}_{\text{tgt}}, x_{\text{ref}}), \quad (1)$$

where $\phi \in \mathbb{R}^{2 \times N}$ in our implementation. Then, a spatial transformation layer S is employed to warp the fully-sampled reference x_{ref} according to the estimated displacement field ϕ . Specifically, in position p , $S(\phi, x_{\text{ref}})[p] = x_{\text{ref}}[p + \phi[p]]$. Finally, the spatially aligned image of the fully-sampled reference $x_{\text{ref}}^A = S(\phi, x_{\text{ref}})$ is fed into the multi-modal reconstruction network together with the under-sampled target modality \bar{x}_{tgt} , and the whole multi-modal MRI reconstruction process becomes

$$\hat{x}_{\text{tgt}} = R_\theta(\bar{x}_{\text{tgt}}, S(\phi, x_{\text{ref}})). \quad (2)$$

Also note that, usually both fully-sampled reference and target images are required to estimate their spatial misalignment. However, in our setting, the fully-sampled target image is not available before reconstruction, thus T_ω takes input of the under-sampled target modality (after zero-filling) instead of the fully-sampled one.

B. Loss Designs

To optimize the spatial alignment network as well as the multi-modal MRI reconstruction network, three loss functions are used in this work. First, the smoothness loss $\mathcal{L}_{\text{smooth}}$ is imposed in favor of a physically reasonable displacement field. Then, the reconstruction loss \mathcal{L}_{rec} asks for high fidelity of the reconstruction result, which also implicitly encourages

accurate spatial alignment between the target and the reference. Finally, the registration loss \mathcal{L}_{reg} is proposed to provide explicit guidance to optimize the spatial alignment network and to contribute to high reconstruction quality.

1) *Smoothness Loss*: It is a common practice to impose smooth prior on the estimated displacement field ϕ in image registration. In our implementation, the smoothness loss is defined as $\mathcal{L}_{\text{smooth}} = \frac{1}{N} \|\nabla \phi\|_2^2$. For 2D MRI, $\mathcal{L}_{\text{smooth}}$ is expanded as

$$\mathcal{L}_{\text{smooth}} = \frac{1}{N} \sum_p \left(\frac{\partial \phi_x}{\partial x} [p] \right)^2 + \left(\frac{\partial \phi_x}{\partial y} [p] \right)^2 + \left(\frac{\partial \phi_y}{\partial x} [p] \right)^2 + \left(\frac{\partial \phi_y}{\partial y} [p] \right)^2. \quad (3)$$

2) *Reconstruction Loss*: The image reconstruction loss \mathcal{L}_{rec} is required to guide the optimization of the reconstruction network R_θ . It is also possible to optimize the spatial alignment network T_ω with the hint from the reconstruction loss, as high-quality reconstruction of the target usually desires for accurate spatial alignment between the two images.

In Fig. 1(b), the reconstruction loss \mathcal{L}_{rec} is applied to the output of the reconstruction network, and its gradient updates both the reconstruction network R_θ and the spatial alignment network T_ω though back-propagation. While it remains an open question to accurately quantify MR image quality, we use the simple pixel-wise 1-norm as the reconstruction loss, i.e., $\mathcal{L}_{\text{rec}} = \|\hat{x}_{\text{tgt}} - x_{\text{tgt}}\|_1$. Note that in most cases, only the magnitudes of MR images are used for diagnosis purpose, thus the phases are ignored during the calculation of the fidelity (e.g., denoting \hat{x}_{tgt} in short of $|\hat{x}_{\text{tgt}}|$ in the above reconstruction loss).

3) *Registration Loss*: Using only the reconstruction loss may not be sufficient to optimize the spatial alignment network, as the back-propagation pathway is too long for the reconstruction loss \mathcal{L}_{rec} to reach the spatial alignment network. As the result, we propose to optimize the spatial alignment network with the direct multi-modal MRI registration loss \mathcal{L}_{reg} , which aims to maximize the similarity between the target and the aligned reference images.

It is challenging though to design image similarity metric especially for multi-modal image registration. Recently, cross-modality image synthesis has provided a new feasible solution to this problem [38]. Instead of directly measuring the similarity between the target x_{tgt} and the aligned reference x_{ref}^A as in Fig. 1(b), we first use the cross-modal synthesis network G_ρ to produce the synthesized target image $x_{\text{ref}}^S = G_\rho(x_{\text{ref}})$. Then, the registration tends to align x_{ref}^S (instead of x_{ref}^A) and produces $x_{\text{ref}}^{\text{SA}} = S(\phi, x_{\text{ref}}^S)$. Next, we can easily calculate $\mathcal{L}_{\text{reg}}^{\text{SA}} = \|\hat{x}_{\text{tgt}} - x_{\text{ref}}^{\text{SA}}\|_1$ and treat it as the dissimilarity between \hat{x}_{tgt} and $x_{\text{ref}}^{\text{SA}}$. Note that the superscript SA indicates the ‘‘synthesis-align (SA)’’ strategy.

The cross-modality synthesis network G_ρ needs to be geometry-preserving. That is, before/after synthesis, the same anatomical structures in the input/output images of G_ρ should be spatially aligned, even though the images are of different modalities in appearance. To this end, we follow Arar *et al.* [39] and use the dual-path registration scheme as in Fig. 2.

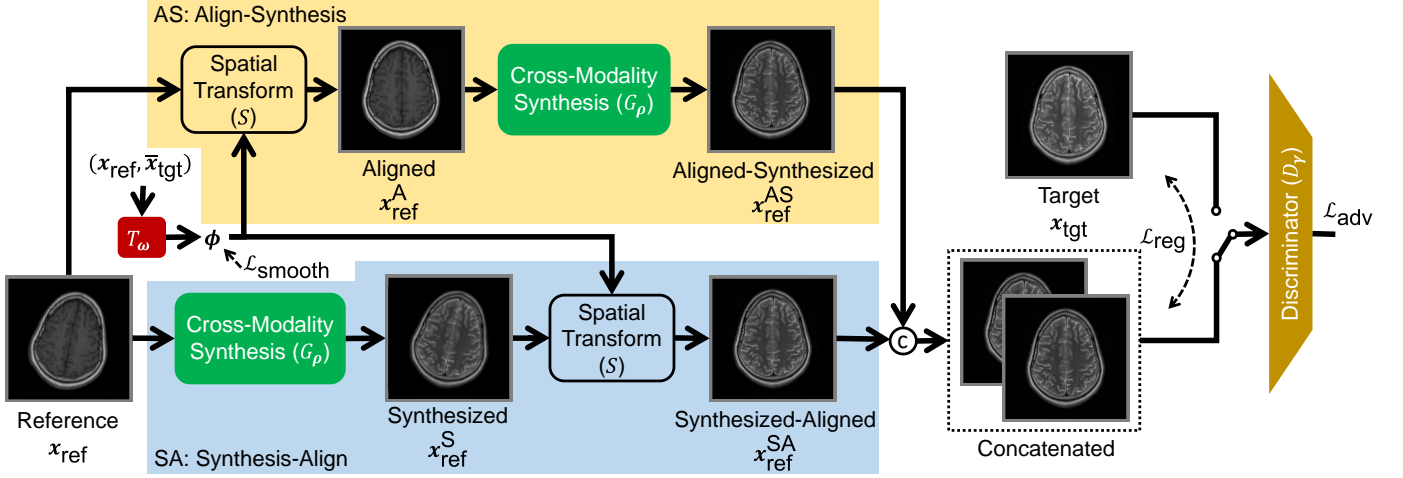


Fig. 2. Illustration of the registration loss \mathcal{L}_{reg} . To measure the cross-modal image similarity between the aligned reference image and the target modality, the cross-modality synthesis network is employed to generate the corresponding target modality from the reference modality. Then we use mono-modality similarity to quantify the difference between the synthesized and real target images. We can either place the synthesis network G_ρ after and before the spatial transform layer S , which derives the align-synthesis (AS) and synthesis-align (SA) branches, respectively. Finally, a discriminator is employed in favor of realistic synthesized images.

Specifically, in addition to the previous introduced loss $\mathcal{L}_{\text{reg}}^{\text{SA}}$, we can place the cross-modality synthesis network after the spatial transform layer. In this way, we can derive the “align-synthesis (AS)” branch (in the top of Fig. 2), which is different with the SA branch in the bottom of the figure. Note that the two branches share the same cross-modality synthesis network parameters. In this way, the final registration loss is a mixture of SA and AS:

$$\mathcal{L}_{\text{reg}} = 0.5 \underbrace{\|x_{\text{tgt}} - x_{\text{ref}}^{\text{SA}}\|_1}_{\text{SA}} + 0.5 \underbrace{\|x_{\text{tgt}} - x_{\text{ref}}^{\text{AS}}\|_1}_{\text{AS}}. \quad (4)$$

The above \mathcal{L}_{reg} also implicitly promotes $x_{\text{ref}}^{\text{SA}} = x_{\text{ref}}^{\text{AS}}$.

C. Implementation Details

In this subsection we introduce more details of our implementation, including the adversarial optimization of the cross-modality synthesis network, and the full algorithm of our multi-modal MRI reconstruction integrated with the spatial alignment network.

1) *Adversarial Loss*: To optimize the cross-modality synthesis network G_ρ , other than the registration loss \mathcal{L}_{reg} , the adversarial loss \mathcal{L}_{adv} is additionally used to encourage more realistic synthesized images. While the registration loss \mathcal{L}_{reg} is 1-norm of the difference between the synthesized and the real target images, the adversarial loss involves a discriminator D_γ that forces the synthesized images to be less distinguishable from the real ones. Following the adversarial training, the generator G_ρ and the discriminator D_γ are optimized alternatively. More specifically, spectral normalization [40] and hinge loss are used. Also, the adversarial loss considers both SA and AS branches as show in Fig. 2:

$$\mathcal{L}_{\text{adv}} = D_\gamma(x_{\text{tgt}}) - 0.5D_\gamma(x_{\text{ref}}^{\text{SA}}) - 0.5D_\gamma(x_{\text{ref}}^{\text{AS}}). \quad (5)$$

The optimization of the cross-modality synthesis network G_ρ and discriminator D_γ can thus be formulated as

$$\rho^*, \gamma^* = \arg \min_{\rho} \max_{\gamma} \mathbb{E}_{p((x_{\text{tgt}}, x_{\text{ref}}))} \alpha \mathcal{L}_{\text{reg}} + \beta \mathcal{L}_{\text{adv}}. \quad (6)$$

2) *Hybrid Supervision over Spatial Alignment Network*: To take advantage of both reconstruction and registration losses towards better spatial aligning and reconstruction quality, the hybrid supervision is imposed on the spatial alignment network. The optimizing of the spatial alignment network solely with the reconstruction loss may be limited due to the long back-propagation pathway, while the direct supervision from only registration loss over the spatial alignment network may deviate from the final goal of high-quality image reconstruction. Thus, with both two loss functions, we combine them as the hybrid supervision upon the spatial alignment network T_ω and the multi-modal reconstruction network R_ρ :

$$\theta^*, \omega^* = \arg \min_{\theta, \omega} \mathbb{E}_{p((x_{\text{tgt}}, x_{\text{ref}}))} \mathcal{L}_{\text{rec}} + \lambda \mathcal{L}_{\text{smooth}} + \alpha \mathcal{L}_{\text{reg}}. \quad (7)$$

The full training scheme of multi-modal reconstruction with spatial alignment network optimized with hybrid reconstruction and registration losses is summarized with following pseudo-code:

Data: Fully sampled multi-modal MR images from same studies, $\{(x_{\text{tgt}}, x_{\text{ref}})\}$.

Output: Optimized neural networks, R_{θ^*} , T_{ω^*} , G_{ρ^*} , and D_{γ^*} .

```

1: repeat
2:    $x_{\text{tgt}}, x_{\text{ref}} \leftarrow p((x_{\text{tgt}}, x_{\text{ref}}))$ 
3:    $\bar{x}_{\text{tgt}} \leftarrow F_{0-\text{fill}}^{-1} F_u x_{\text{tgt}}$ 
4:    $\phi \leftarrow T_\omega(\bar{x}_{\text{tgt}}, x_{\text{ref}})$ 
5:    $\hat{x}_{\text{tgt}} \leftarrow R_\theta(\bar{x}_{\text{tgt}}, S(\phi, x_{\text{ref}}))$ 
6:    $x_{\text{ref}}^{\text{SA}}, x_{\text{ref}}^{\text{AS}} \leftarrow S(\phi, G_\rho(x_{\text{ref}})), G_\rho(S(\phi, x_{\text{ref}}))$ 
7:    $\mathcal{L}_{\text{smooth}} \leftarrow \frac{1}{N} \|\nabla \phi\|_2^2$ 
8:    $\mathcal{L}_{\text{rec}} \leftarrow \|\hat{x}_{\text{tgt}} - x_{\text{tgt}}\|_1$ 
9:    $\mathcal{L}_{\text{adv}} \leftarrow D_\gamma(x_{\text{tgt}}) - 0.5D_\gamma(x_{\text{ref}}^{\text{SA}}) - 0.5D_\gamma(x_{\text{ref}}^{\text{AS}})$ 
10:   $\mathcal{L}_{\text{reg}} \leftarrow 0.5\|x_{\text{tgt}} - x_{\text{ref}}^{\text{SA}}\|_1 + 0.5\|x_{\text{tgt}} - x_{\text{ref}}^{\text{AS}}\|_1$ 
11:   $\theta \leftarrow \theta - \eta \partial_\theta \mathcal{L}_{\text{rec}}$ 
12:   $\omega \leftarrow \omega - \eta \partial_\omega (\mathcal{L}_{\text{rec}} + \lambda \mathcal{L}_{\text{smooth}} + \alpha \mathcal{L}_{\text{reg}})$ 
13:   $\rho \leftarrow \rho - \eta \partial_\rho (\alpha \mathcal{L}_{\text{reg}} + \beta \mathcal{L}_{\text{adv}})$ 
14:   $\gamma \leftarrow \gamma + \eta \partial_\gamma (\beta \mathcal{L}_{\text{adv}})$ 

```

15: **until** convergence

where λ , α , and β are the weights for $\mathcal{L}_{\text{smooth}}$, \mathcal{L}_{reg} , and \mathcal{L}_{adv} , and η is the learning rate.

Hyper-parameters are selected with rule of thumb without much tuning for robust demonstration. In our implementation, large weight ($\lambda = 100$) is used for the smoothness loss $\mathcal{L}_{\text{smooth}}$ for intra-subject registration. For synthesis-based image registration loss \mathcal{L}_{reg} , we simply assign it the same importance with the reconstruction loss \mathcal{L}_{rec} i.e. $\alpha = 1.0$. Moreover, the weight for the adversarial loss \mathcal{L}_{adv} is set to $\beta = 0.1$, and a smaller β may lead to unstable adversarial training.

IV. EXPERIMENTS

Two sets of experiments are conducted on MRI with and without raw k -space data. The MR images without raw acquisition are recompiled from the large and publicly accessible fastMRI dataset [41], [42], while the MR images with raw multi-coil k -space data are collected from our in-house MRI dataset. For MR images from the fastMRI dataset, we use DICOM (digital imaging and communications in medicine) data that are scanned in real clinical settings, thus the misalignment between sequences is more representative than those acquired in the purpose of basic research.

Our implementation is mainly based on PyTorch library and the neural networks are trained on Nvidia 1080Ti GPUs. The Adam optimizer with learning rate of $\eta = 0.0001$ and batch size of 4 are used. Also, the early-stop strategy of 50,000 iterations, which costs about 6 hours with our hybrid optimization, is used to prevent over-fitting. Considering all MR images are scanned with large slice spacing and thickness, 2D slices are extracted from 3D volumes for training and evaluation. The code is publicly available at <https://github.com/woxuankai/SpatialAlignmentNetwork> to help the reproduction of our work.

In both experiments, following the paradigm of fastMRI, the under-sampled MRI is acquired by down-sampling the corresponding fully-sampled version in k -space with a pre-defined sampling pattern satisfying with the constraint of Cartesian sampling trajectories. More specifically, two typical sampling patterns - the random and equispaced sampling patterns - are used in our experiments, with a sampling ratio of 25% or 12.5%, respectively. Considering the fact that the low frequency signals contain most of the energy in the k -space, for both random and equispaced patterns, 32% of the samplings are always allocated to the lowest frequencies, while the rest samplings are distributed randomly or equally-spaced. The under-sampling patterns used in the experiments on fastMRI DICOM are show in Fig. 3.

Also, the ResNet, with batch normalization removed and global residual connection added for better performance, is employed as the reconstruction network backbone, and a U-Net which is similar to that used in Balakrishnan *et al.* [32] is used as our spatial alignment network. More implementation details can be found in the released code.

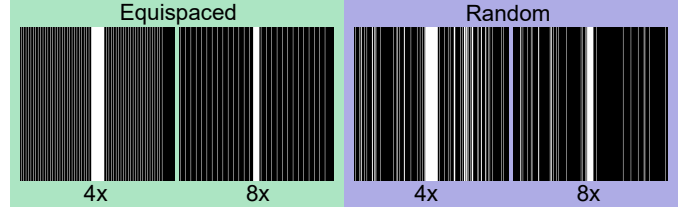


Fig. 3. The under-sampling k -space patterns used in the experiments on fastMRI DICOM dataset. The numbers in the bottom of individual patterns indicate the acceleration factors.

A. Experiments on fastMRI DICOM

We first run our proposed method on brain MRI collected from anonymous DICOM of the open fastMRI dataset. The multi-modal MRI is not explicitly provided by fastMRI. Thus the data used in this subsection are recompiled by iterating over all studies in the repository and selecting only those with T1- and T2-weighted brain MRI with same geometry scanned in axial planes. After that, a total of 340 pairs of T1- and T2-weighted MR images are extracted. Among them, 238 volume pairs (3808 slices) are used for training, and 102 volume pairs (1632 slice pairs) for testing. For both T1- and T2-weighted images, the in-plane size is 320×320 , the resolution is $0.68 \text{ mm} \times 0.68 \text{ mm}$, and the slice spacing is 5 mm. In our experiments, following Xiang *et al.* [4], the fully-sampled T1-weighted MRI is used to help the reconstruction of T2-weighted image, with 25% under-sampling ratio ($4 \times$ Acceleration) and 12.5% under-sampling ratio ($8 \times$ Acceleration) in random and equispaced under-sampling patterns (cf. Fig. 3).

Table I compares the multi-modal MRI reconstruction with different settings and methods. Particularly, “ResNet” is the baseline multi-modal reconstruction without spatial aligning, while “Reg”, “Rec”, and “Rec-Reg” are for multi-modal reconstruction with the spatial alignment network integrated. Among them, the training loss for the reconstruction network are the same, but the spatial alignment network is optimized with different loss functions. More specifically, aside from the smoothness loss \mathcal{L}_{rec} , in Reg, the spatial alignment network is trained with the registration loss \mathcal{L}_{reg} only; in Rec, the spatial alignment network is trained with the reconstruction loss \mathcal{L}_{rec} only; and in Rec-Reg, the spatial alignment network is trained with both registration and reconstruction losses (i.e., $\mathcal{L}_{\text{rec}} + \mathcal{L}_{\text{reg}}$).

It is obvious that multi-modal MRI reconstruction (Reg, Rec, and Rec-Reg) with spatial alignment network performs significantly better ($p < 0.01$ with paired t -tests) than the method without spatially aligning (ResNet) in both PSNR (peak signal-to-noise ratio, the higher the better) and SSIM (structural similarity, the higher the better) in all settings. Also, among the methods with the spatial alignment network enabled, the hybrid optimization strategy with both reconstruction and registration losses (Rec-Reg) turns better than the optimization with only the registration loss (Reg) or with the single reconstruction loss (Rec).

To better demonstrate the superiority of the proposed method, the subject-wise PSNR/SSIM gain (i.e., between Reg,

TABLE I

QUANTITATIVE COMPARISON ON RECONSTRUCTION RESULTS OF THE FASTMRI DICOM DATASET. UNDER-SAMPLED T2-WEIGHTED MRI IS RECONSTRUCTED WITH HELPS OF FULLY-SAMPLED T1-WEIGHTED IMAGE. IN ALL SETTINGS AND METRICS, PERFORMANCES SIGNIFICANTLY GET BETTER WHEN EMPOWERED WITH THE SPATIAL ALIGNMENT NETWORK (REG/REC/REC-REG VS. RESNET, $p < 0.01$ WITH PAIRED t -TESTS).

		4× Acceleration		8× Acceleration	
		PSNR	SSIM	PSNR	SSIM
Equispaced	ResNet	37.46 ±1.87	0.9708 ±0.0101	35.21 ±1.89	0.9591 ±0.0140
	Reg	37.73 ±1.76	0.9722 ±0.0090	35.65 ±1.82	0.9621 ±0.0126
	Rec	37.94 ±1.88	0.9732 ±0.0092	35.96 ±1.97	0.9639 ±0.0129
	Rec-Reg	38.11 ±1.84	0.9737 ±0.0089	36.11 ±1.95	0.9648 ±0.0124
Random	ResNet	38.10 ±1.67	0.9732 ±0.0081	34.15 ±1.92	0.9517 ±0.0167
	Reg	38.30 ±1.60	0.9739 ±0.0076	34.66 ±1.85	0.9557 ±0.0147
	Rec	38.49 ±1.73	0.9751 ±0.0077	34.82 ±1.86	0.9570 ±0.0141
	Rec-Reg	38.70 ±1.69	0.9756 ±0.0074	34.93 ±1.86	0.9578 ±0.0140

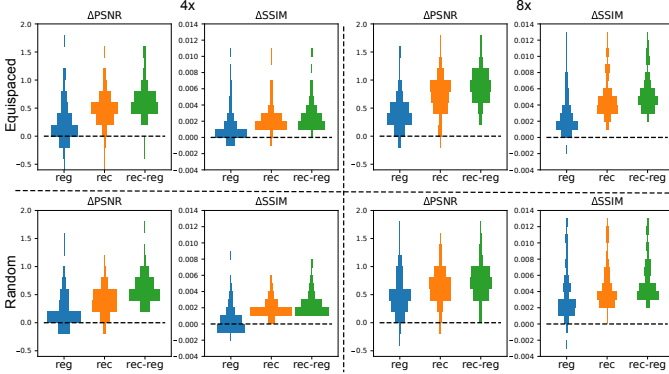


Fig. 4. Performance improvement (in PSNR/SSIM) from the spatial alignment network with different optimization strategies over multi-modal reconstruction without spatial aligning on fastMRI DICOM dataset.

Rec, Rec-Reg individually and ResNet) is shown in detailed histograms of Fig. 4. For the spatial alignment network optimized with the registration loss only (Reg), although the overall performance gain is positive as in Table I, quite a number of subjects (41.2% for all settings and metrics) are unfortunately negative in terms of reduced PSNR/SSIM after the spatial alignment network is added. For those using the reconstruction loss only (Rec), the results are much better as most of the subjects (96.1% among varying settings and metrics) achieve positive performance gain. Finally, with the proposed method (Rec-Reg), the performance of all subjects is better than that without any spatial aligning (ResNet), except for an 2 outlier subjects (about 2%) with 4× Equispaced sampling pattern and PSNR metric. The results indicate that the proposed method is not only superior in quantitative metrics but also robust for nearly all subjects.

Further, visual comparison of the reconstruction quality is provided in Fig. 5, and the target modality can be better reconstructed when the spatial alignment network is integrated. For

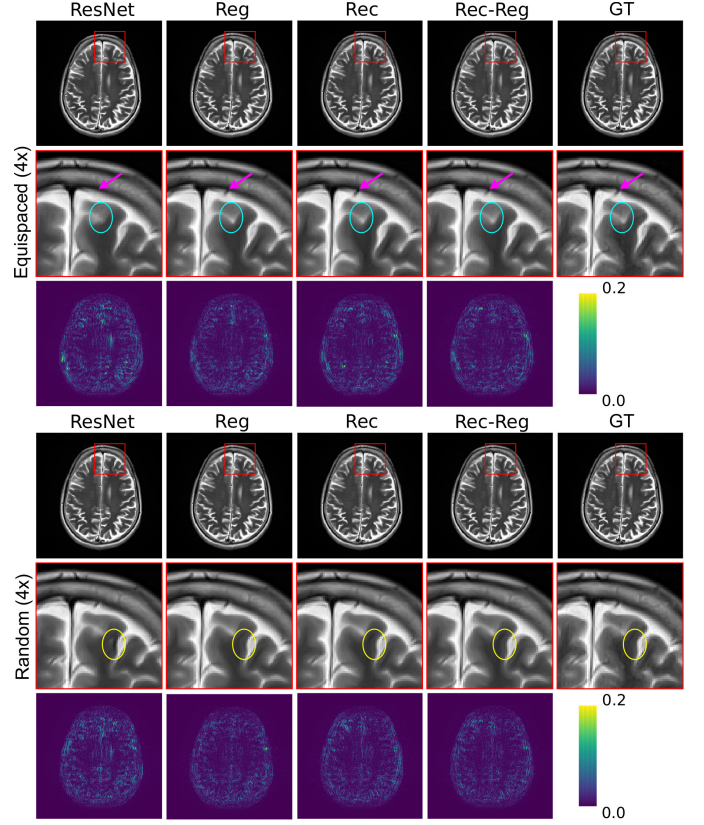


Fig. 5. Visual comparison of the reconstructed target MR images on fastMRI DICOM dataset. Results of equispaced and random under-sampling patterns at 4× acceleration ratio are compared. The first and the fourth rows are for the reconstructed images, with red bounding-boxes zoomed-in in the second and the fifth rows. The corresponding error maps are provided in the third and the sixth rows, respectively.

example, low intensities in cerebrospinal fluid (CSF) (pointed by magenta arrow near prefrontal cortex) are missing in the MR image reconstructed without spatial alignment (ResNet), and the CSF / gray matter (GM) boundary (in cyan circle) is fuzzy. Instead, when powered with the spatial alignment network, the edges of GM are sharper, specifically the white matter (WM) / GM boundary highlighted by yellow circles. The error maps, by subtracting the reconstructed target images with the ground-truth, are also consistent with the quantitative comparison in Table I, as the errors decrease after the spatial alignment network is integrated.

It is also necessary to explore the displacement fields generated by the spatial alignment network. Fig. 6 shows the displacement fields and the warped reference images accordingly. The two rows on the bottom are the fully-sampled target image and the ground-truth reference modality in checkerboard. In the zoomed-in views (last row), the spatial misalignment between the two modalities is clearly visible, in that the boundary of the skull is inconsistent (pointed by green arrows) and discontinuity exists in brain center-line (pointed by red arrows). On the top in Fig. 6, we show the estimated displacement fields and the corresponding aligned reference images. Different settings for training the spatial alignment network are illustrated by different columns, in the consistent way with Table I. Particularly, the displacements

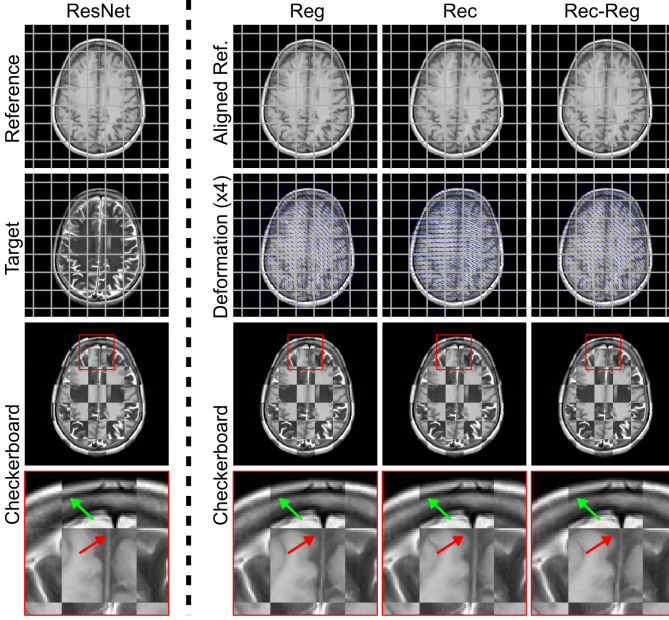


Fig. 6. Effects of spatial alignment network. The original target and reference images are shown in checkerboard and zoomed-in in the first two columns. The estimated displacement and the aligned reference images are in the third and fourth columns, respectively. Different rows are for individual ways to implement the spatial alignment network. Note the displacement fields are amplified by four times for better visualization.

are amplified for a factor of 4 and rendered in blue arrows for clear illustration. In both Reg and Rec-Reg, the reference image can be well aligned with the target modality visually, while Rec is less accurate in aligning brain centerline (pointed by red arrows as in the last row of the figure). The comparisons underscore our argument that the long-way back-propagated from the reconstruction loss can be insufficient to optimize the spatial alignment network. We also note that, given the example in Fig. 6, the reference image and the target image appear to have a subtle rotation in the anti-clockwise direction, which can be attributed to unexpected motion of the subject.

B. Experiments on MRI with k -space Data

In this subsection, we conduct experiments on a private set of 24-channel 3T MR images with raw k -space data. We collect a total of 62 studies, where each study contains paired T1-weighted fluid-attenuated inversion recovery (T1-FLAIR, $TR = 2015\text{ms}$ and $TE = 12\text{ms}$) and T2-weighted ($TR = 4226\text{ms}$ and $TE = 104.8\text{ms}$) MRI. Again, 2D slices, with spatial size of 320×320 , spacing of $0.7\text{mm} \times 0.7\text{mm}$ and slice thickness of 5mm , are extracted from individual volumes. More specifically, 31 subjects (627 slices) are used for training, and the rest 31 subjects (621 slices) are for testing. Following fastMRI, the ground-truth images are virtual single-coil data combined from multi-coil MRI by root-sum-of-squares (RSS). Considering the limited number of training data, paired BSpline data augmentation (i.e., to augment target and reference MRI with the same BSpline-based displacement fields) is used for training.

Quantitative comparison of different reconstruction methods in varying settings can be found in TABLE II, in a similar way

TABLE II
QUANTITATIVE COMPARISON OF THE RECONSTRUCTION RESULTS OF THE PRIVATE MULTI-COIL MRI DATASET WITH REAL k -SPACE DATA. UNDER-SAMPLED T2-WEIGHTED MRI IS RECONSTRUCTED WITH HELPS OF FULLY-SAMPLED T1-FLAIR IMAGE. AGAIN, IN ALL SETTINGS AND METRICS, PERFORMANCES SIGNIFICANTLY GET BETTER WHEN EMPOWERED WITH THE SPATIAL ALIGNMENT NETWORK (REG/REC/REC-REG VS. RESNET, $p < 0.01$ WITH PAIRED t -TESTS).

		4 \times Acceleration		8 \times Acceleration	
		PSNR	SSIM	PSNR	SSIM
Equispaced	ResNet	40.02 ± 0.71	0.9715 ± 0.0046	36.05 ± 0.66	0.9507 ± 0.0073
	Reg	40.07 ± 0.68	0.9717 ± 0.0043	36.64 ± 0.66	0.9550 ± 0.0061
	Rec	40.56 ± 0.72	0.9739 ± 0.0042	37.43 ± 0.63	0.9596 ± 0.0055
	Rec-Reg	40.64 ± 0.70	0.9741 ± 0.0040	37.45 ± 0.62	0.9597 ± 0.0054
Random	ResNet	38.59 ± 0.69	0.9660 ± 0.0050	34.70 ± 0.70	0.9414 ± 0.0089
	Reg	38.78 ± 0.66	0.9676 ± 0.0042	35.47 ± 0.60	0.9478 ± 0.0065
	Rec	39.09 ± 0.69	0.9676 ± 0.0049	35.81 ± 0.61	0.9497 ± 0.0064
	Rec-Reg	39.25 ± 0.68	0.9685 ± 0.0045	36.25 ± 0.62	0.9524 ± 0.0060

with the experiments on fastMRI DICOM dataset. Compared to conventional multi-modal MRI reconstruction (ResNet), the methods with spatial alignment (Reg, Rec, and Rec-Reg) perform generally better ($p < 0.01$ with paired t -tests). Among them, the hybrid optimization strategy (Rec-Reg) achieves the best performance in both PSNR and SSIM, while the results of spatial alignment trained with solely the registration loss (Reg) or the reconstruction loss (Rec) vary in different settings.

Fig. 7 visually illustrates the reconstruction results and corresponding error maps of T2-weighted MRI under-sampled with the random sampling pattern at $4\times$ acceleration ratio. The corresponding T1-FLAIR MRI is used as the reference modality. For multi-modal MRI reconstruction without the spatial alignment network, apparently artifacts (pointed by yellow arrows) exist in the reconstructed image. With the spatial alignment network optimized with solely the reconstruction or the registration loss, the artifacts are much reduced. And the image quality gets further improved with both reconstruction and registration losses enabled.

Also, to visualize the reduced spatial misalignment, Fig. 8 shows the target modality, as well as both the original and aligned reference MRI. The checkerboard observes obvious discontinuity of the anatomical structures, which is evidence of the spatial misalignment. With the spatial alignment network optimized with the reconstruction loss only (Rec), such discontinuity is much mitigated. That is, although the two images may not be perfectly aligned, the idea of the reconstruction-loss-driven optimization is feasible. With the spatial alignment network optimized with the registration loss (Reg) or hybrid training (Rec-Reg), the discontinuity in the checkerboard image is visually imperceptible, which means the spatial misalignment between the target and reference images is well-fixed.

Fig. 8 shows the estimated displacement fields aligning the reference modality with the target modality. For Reg or Rec-

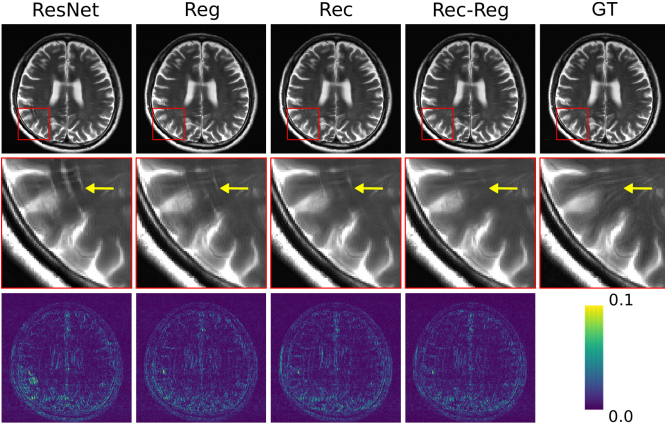


Fig. 7. Visual comparison of reconstructed images, zoomed-in views, and error maps on the private multi-coil raw k -space dataset. T1-FLAIR MR images are used to help the reconstruction of T2-weighted MRI under-sampled with random under-sampling pattern at $4\times$ acceleration ratio.

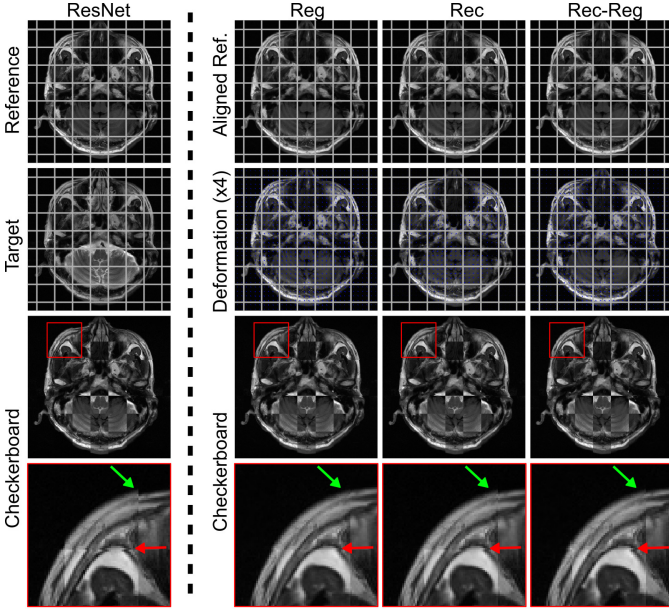


Fig. 8. Effects of spatial alignment network on MRI with multi-coil raw k -space data. T1-FLAIR MR images are used to help the reconstruction of T2-weighted MRI. The displacement fields are amplified by a factor of 4 for better visualization.

Reg, the orientations of the estimated displacement fields are largely the same. Contrarily, the displacement fields of Rec are very different, with the displacement vectors pointing at various directions which is not reasonable in fact. To this end, we argue that such low-quality displacement field can also partially illustrate the relatively weak guidance provided by solely the reconstruction loss.

V. DISCUSSION AND CONCLUSION

In this manuscript, to deal with the subtle spatial misalignment between MRI sequences, which is unfortunately prevalent even in the same study, we propose to explicitly align the reference modality with the target modality, and feed them together to the deep network for reconstruction.

More specifically, the spatial alignment network takes fully-sampled reference MRI and under-sampled target image as the input and outputs the displacement field to align the reference modality. Also, a hybrid optimization strategy is proposed to provide strong training supervision for the spatial alignment network. Experiments on both clinical DICOM data and multi-coil raw k -space data demonstrate that the spatial alignment network not only improves overall reconstruction performance quantitatively and qualitatively, but also is robust as it brings performance gain to almost all subjects. The proposed spatial alignment network is flexible and theoretically it can be plug-in to any multi-modal reconstruction network.

Further research directions include extending the spatial alignment network to more organs and 3D MR images, while in this manuscript we only use 2D aligning due to large slice thickness. Also, the spatial alignment is promising at improving the performance of joint reconstruction of multiple (≥ 3) MRI sequences due to the highly flexible learning-based alignment network with deformable transformations. Finally, recurrently aligning different sequences is also interesting as MRI reconstruction with recurrent neural networks fits the iterative nature of the optimization algorithms.

REFERENCES

- [1] K. P. Pruessmann, M. Weiger, M. B. Scheidegger, and P. Boesiger, "SENSE: Sensitivity encoding for fast MRI," *Magnetic Resonance in Medicine*, vol. 42, no. 5, pp. 952–962, 1999.
- [2] M. A. Griswold, P. M. Jakob, R. M. Heidemann, M. Nittka, V. Jellus, J. Wang, B. Kiefer, and A. Haase, "Generalized autocalibrating partially parallel acquisitions (GRAPPA)," *Magnetic Resonance in Medicine*, vol. 47, no. 6, pp. 1202–1210, 2002.
- [3] M. Lustig, D. Donoho, and J. M. Pauly, "Sparse MRI: The application of compressed sensing for rapid MR imaging," *Magnetic Resonance in Medicine*, vol. 58, no. 6, pp. 1182–1195, 2007.
- [4] L. Xiang, Y. Chen, W. Chang, Y. Zhan, W. Lin, Q. Wang, and D. Shen, "Ultra-Fast T2-Weighted MR Reconstruction Using Complementary T1-Weighted Information," in *Medical Image Computing and Computer Assisted Intervention - MICCAI 2018*, ser. Lecture Notes in Computer Science, A. F. Frangi, J. A. Schnabel, C. Davatzikos, C. Alberola-Lopez, and G. Fichtinger, Eds. Springer International Publishing, 2018, pp. 215–223.
- [5] K. H. Kim, W.-J. Do, and S.-H. Park, "Improving resolution of MR images with an adversarial network incorporating images with different contrast," *Medical Physics*, vol. 45, no. 7, pp. 3120–3131, 2018.
- [6] Z. Lai, X. Qu, H. Lu, X. Peng, D. Guo, Y. Yang, G. Guo, and Z. Chen, "Sparse MRI reconstruction using multi-contrast image guided graph representation," *Magnetic Resonance Imaging*, vol. 43, pp. 95–104, Nov. 2017.
- [7] L. Xiang, Y. Chen, W. Chang, Y. Zhan, W. Lin, Q. Wang, and D. Shen, "Deep-Learning-Based Multi-Modal Fusion for Fast MR Reconstruction," *IEEE Transactions on Biomedical Engineering*, vol. 66, no. 7, pp. 2105–2114, Jul. 2019.
- [8] B. Zhou and S. K. Zhou, "DuDoRNet: Learning a Dual-Domain Recurrent Network for Fast MRI Reconstruction With Deep T1 Prior," in *2020 IEEE/CVF Conference on Computer Vision and Pattern Recognition (CVPR)*, Jun. 2020, pp. 4272–4281, iSSN: 2575-7075.
- [9] Q. Lyu, H. Shan, C. Steber, C. Helis, C. Whitlow, M. Chan, and G. Wang, "Multi-Contrast Super-Resolution MRI Through a Progressive Network," *IEEE Transactions on Medical Imaging*, vol. 39, no. 9, pp. 2738–2749, Sep. 2020, conference Name: IEEE Transactions on Medical Imaging.
- [10] S. U. Dar, M. Yurt, M. Shahdloo, M. E. Ildiz, B. Tinaz, and T. Cukur, "Prior-Guided Image Reconstruction for Accelerated Multi-Contrast MRI via Generative Adversarial Networks," *IEEE Journal of Selected Topics in Signal Processing*, vol. 14, no. 6, pp. 1072–1087, Oct. 2020.
- [11] L. Sun, Z. Fan, X. Fu, Y. Huang, X. Ding, and J. Paisley, "A Deep Information Sharing Network for Multi-Contrast Compressed Sensing MRI Reconstruction," *IEEE Transactions on Image Processing*, vol. 28,

- no. 12, pp. 6141–6153, Dec. 2019, conference Name: IEEE Transactions on Image Processing.
- [12] D. L. Donoho, “Compressed sensing,” *IEEE Transactions on Information Theory*, vol. 52, no. 4, pp. 1289–1306, Apr. 2006.
 - [13] S. Wang, Z. Su, L. Ying, X. Peng, S. Zhu, F. Liang, D. Feng, and D. Liang, “Accelerating magnetic resonance imaging via deep learning,” in *2016 IEEE 13th International Symposium on Biomedical Imaging (ISBI)*, Apr. 2016, pp. 514–517, iSSN: 1945-8452.
 - [14] J. Schlemper, J. Caballero, J. V. Hajnal, A. N. Price, and D. Rueckert, “A Deep Cascade of Convolutional Neural Networks for Dynamic MR Image Reconstruction,” *IEEE Transactions on Medical Imaging*, vol. 37, no. 2, pp. 491–503, Feb. 2018.
 - [15] C. Qin, J. Schlemper, J. Caballero, A. N. Price, J. V. Hajnal, and D. Rueckert, “Convolutional Recurrent Neural Networks for Dynamic MR Image Reconstruction,” *IEEE Transactions on Medical Imaging*, vol. 38, no. 1, pp. 280–290, Jan. 2019.
 - [16] Y. Han, L. Sunwoo, and J. C. Ye, “\$k\$-Space Deep Learning for Accelerated MRI,” *IEEE Transactions on Medical Imaging*, vol. 39, no. 2, pp. 377–386, Feb. 2020.
 - [17] Y. Zhang, P.-T. Yap, L. Qu, J.-Z. Cheng, and D. Shen, “Dual-domain convolutional neural networks for improving structural information in 3 T MRI,” *Magnetic Resonance Imaging*, vol. 64, pp. 90–100, Dec. 2019.
 - [18] B. Zhu, J. Z. Liu, S. F. Cauley, B. R. Rosen, and M. S. Rosen, “Image reconstruction by domain-transform manifold learning,” *Nature*, vol. 555, no. 7697, pp. 487–492, Mar. 2018.
 - [19] R. Souza, Y. Beauferris, W. Loos, R. M. Lebel, and R. Frayne, “Enhanced Deep-Learning-Based Magnetic Resonance Image Reconstruction by Leveraging Prior Subject-Specific Brain Imaging: Proof-of-Concept Using a Cohort of Presumed Normal Subjects,” *IEEE Journal of Selected Topics in Signal Processing*, vol. 14, no. 6, pp. 1126–1136, Oct. 2020.
 - [20] L. Weizman, Y. C. Eldar, and D. B. Bashat, “Compressed sensing for longitudinal MRI: An adaptive-weighted approach,” *Medical Physics*, vol. 42, no. 9, pp. 5195–5208, 2015.
 - [21] —, “Reference-based MRI,” *Medical Physics*, vol. 43, no. 10, pp. 5357–5369, 2016.
 - [22] A. Hirabayashi, N. Inamuro, K. Mimura, T. Kurihara, and T. Homma, “Compressed sensing MRI using sparsity induced from adjacent slice similarity,” in *2015 International Conference on Sampling Theory and Applications (SampTA)*, May 2015, pp. 287–291.
 - [23] L. Xiang, Y. Qiao, D. Nie, L. An, W. Lin, Q. Wang, and D. Shen, “Deep auto-context convolutional neural networks for standard-dose PET image estimation from low-dose PET/MRI,” *Neurocomputing*, vol. 267, pp. 406–416, Dec. 2003.
 - [24] A. Majumdar and R. K. Ward, “Joint reconstruction of multiecho MR images using correlated sparsity,” *Magnetic Resonance Imaging*, vol. 29, no. 7, pp. 899–906, Sep. 2011.
 - [25] J. Huang, C. Chen, and L. Axel, “Fast multi-contrast MRI reconstruction,” *Magnetic Resonance Imaging*, vol. 32, no. 10, pp. 1344–1352, Dec. 2014.
 - [26] P. Song, L. Weizman, J. F. C. Mota, Y. C. Eldar, and M. R. D. Rodrigues, “Coupled Dictionary Learning for Multi-Contrast MRI Reconstruction,” *IEEE Transactions on Medical Imaging*, vol. 39, no. 3, pp. 621–633, Mar. 2020.
 - [27] B. B. Avants, C. L. Epstein, M. Grossman, and J. C. Gee, “Symmetric diffeomorphic image registration with cross-correlation: Evaluating automated labeling of elderly and neurodegenerative brain,” *Medical Image Analysis*, vol. 12, no. 1, pp. 26–41, Feb. 2008.
 - [28] J. P. Thirion, “Image matching as a diffusion process: an analogy with Maxwell’s demons,” *Medical Image Analysis*, vol. 2, no. 3, pp. 243–260, Sep. 1998.
 - [29] T. Vercauteren, X. Pennec, A. Perchant, and N. Ayache, “Diffeomorphic demons: Efficient non-parametric image registration,” *NeuroImage*, vol. 45, no. 1, Supplement 1, pp. S61–S72, Mar. 2009.
 - [30] P. Hellier, J. Ashburner, I. Corouge, C. Barillot, and K. J. Friston, “Inter-subject Registration of Functional and Anatomical Data Using SPM,” in *Medical Image Computing and Computer-Assisted Intervention - MICCAI 2002*, ser. Lecture Notes in Computer Science, T. Dohi and R. Kikinis, Eds. Berlin, Heidelberg: Springer, 2002, pp. 590–597.
 - [31] X. Yang, R. Kwitt, M. Styner, and M. Niethammer, “Quicksilver: Fast predictive image registration - A deep learning approach,” *NeuroImage*, vol. 158, pp. 378–396, Sep. 2017.
 - [32] G. Balakrishnan, A. Zhao, M. R. Sabuncu, A. V. Dalca, and J. Guttag, “An Unsupervised Learning Model for Deformable Medical Image Registration,” in *2018 IEEE/CVF Conference on Computer Vision and Pattern Recognition*, Jun. 2018, pp. 9252–9260.
 - [33] P. Thevenaz and M. Unser, “Optimization of mutual information for multiresolution image registration,” *IEEE Transactions on Image Processing*, vol. 9, no. 12, pp. 2083–2099, Dec. 2000.
 - [34] D. Mattes, D. R. Haynor, H. Vesselle, T. K. Lewellen, and W. Eubank, “PET-CT image registration in the chest using free-form deformations,” *IEEE Transactions on Medical Imaging*, vol. 22, no. 1, pp. 120–128, Jan. 2003.
 - [35] S. M. Smith, M. Jenkinson, M. W. Woolrich, C. F. Beckmann, T. E. J. Behrens, H. Johansen-Berg, P. R. Bannister, M. De Luca, I. Drobnjak, D. E. Flitney, R. K. Niazy, J. Saunders, J. Vickers, Y. Zhang, N. De Stefano, J. M. Brady, and P. M. Matthews, “Advances in functional and structural MR image analysis and implementation as FSL,” *NeuroImage*, vol. 23, pp. S208–S219, Jan. 2004.
 - [36] M. P. Heinrich, M. Jenkinson, M. Bhushan, T. Matin, F. V. Gleeson, S. M. Brady, and J. A. Schnabel, “MIND: Modality independent neighbourhood descriptor for multi-modal deformable registration,” *Medical Image Analysis*, vol. 16, no. 7, pp. 1423–1435, Oct. 2012.
 - [37] J. Fan, X. Cao, Q. Wang, P.-T. Yap, and D. Shen, “Adversarial learning for mono- or multi-modal registration,” *Medical Image Analysis*, vol. 58, p. 101545, Dec. 2019.
 - [38] X. Cao, J. Yang, Y. Gao, Q. Wang, and D. Shen, “Region-adaptive deformable registration of ct/mri pelvic images via learning-based image synthesis,” *IEEE Transactions on Image Processing*, vol. 27, no. 7, pp. 3500–3512, 2018.
 - [39] M. Arar, Y. Ginger, D. Danon, A. H. Bermanno, and D. Cohen-Or, “Unsupervised Multi-Modal Image Registration via Geometry Preserving Image-to-Image Translation,” in *2020 IEEE/CVF Conference on Computer Vision and Pattern Recognition (CVPR)*, Jun. 2020, pp. 13 407–13 416, iSSN: 2575-7075.
 - [40] T. Miyato, T. Kataoka, M. Koyama, and Y. Yoshida, “Spectral Normalization for Generative Adversarial Networks,” in *International Conference on Learning Representations*, Feb. 2018.
 - [41] J. Zbontar, F. Knoll, A. Sriram, T. Murrell, Z. Huang, M. J. Muckley, A. Defazio, R. Stern, P. Johnson, M. Bruno, M. Parente, K. J. Geras, J. Katsnelson, H. Chandarana, Z. Zhang, M. Drozdal, A. Romero, M. Rabbat, P. Vincent, N. Yakubova, J. Pinkerton, D. Wang, E. Owens, C. L. Zitnick, M. P. Recht, D. K. Sodickson, and Y. W. Lui, “fastMRI: An Open Dataset and Benchmarks for Accelerated MRI,” *arXiv:1811.08839 [physics, stat]*, Dec. 2019, arXiv: 1811.08839.
 - [42] F. Knoll, J. Zbontar, A. Sriram, M. J. Muckley, M. Bruno, A. Defazio, M. Parente, K. J. Geras, J. Katsnelson, H. Chandarana, Z. Zhang, M. Drozdal, A. Romero, M. Rabbat, P. Vincent, J. Pinkerton, D. Wang, N. Yakubova, E. Owens, C. L. Zitnick, M. P. Recht, D. K. Sodickson, and Y. W. Lui, “fastMRI: A Publicly Available Raw k-Space and DICOM Dataset of Knee Images for Accelerated MR Image Reconstruction Using Machine Learning,” *Radiology: Artificial Intelligence*, vol. 2, no. 1, p. e190007, Jan. 2020.